Radiation Measurements 168 (2023) 107001

Contents lists available at ScienceDirect

Radiation Measurements

journal homepage: www.elsevier.com/locate/radmeas

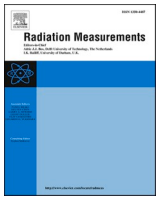

Quantitative beta autoradiography of a heterogeneous granulite sample and implications for luminescence dating

L. Martin [a,b,*], D.C.W. Sanderson [a], S. Paling [c], A. Cresswell [a], S.K. Fitzgerald [a]

[a] Scottish Universities Environmental Research Centre, Glasgow, United Kingdom
[b] Royal Society Newton International Fellow, United Kingdom
[c] Boulby Underground Laboratory, Saltburn-by-the-Sea, United Kingdom

ARTICLE INFO

Keywords:
Luminescence
Autoradiography
Rocks
Beta dose rate
Modelling
Imaging

ABSTRACT

Beta dose rate heterogeneity is a known source of scatter in OSL measurement and equivalent dose distributions. Without proper methods to describe and account for it, it can contribute significantly to the uncertainties in OSL ages. For this reason, investigating the beta dose rate (β Dr) distribution is necessary to improve the dating of heterogeneous samples. Here we present a method for quantitative and high sensitivity autoradiographic imaging of beta dose rates. It is demonstrated using highly heterogeneous granulite rock samples. The accuracy and sensitivity of this method is improved using pulsed laser stimulation, and by underground exposure of samples in an ultra-low background environment. Results are calibrated using gamma (γ)irradiation and Monte Carlo simulation and have been validated using homogeneous dose rate standards. Combining analysis of autoradiography results and SEM backscattered images of the same samples allows determination of the dose rate distributions in the different mineral phases. A significant difference between the dose rate of K-feldspar grains obtained from the imaging and the dose rates calculated using methods commonly used in OSL dating is noted because of the clustering of grains in the sample. This represents a risk of bias in age determination in coarse grained rock samples which can be analysed using dose rate imaging methods. The beta Dr spatial distributions result in a significant dose scattering received by single grains, even compared to the total dose rate. The effect of such beta dose rate distributions on OSL dating of coarse-grained crystalline materials is discussed.

1. Introduction

Beta dose rate (β Dr) heterogeneity has been recognized for long as a potential source of luminescence measurement scattering in sediment, potentially contributing to the dispersion of Thermoluminescence (TL) (Scott and Sanderson, 1988; Sanderson et al., 1988) and Optically Stimulated Luminescence (OSL) dating results (Murray and Roberts, 1997; Nathan et al., 2003). However, precise quantitative measurement of the spatial variations of β Dr at natural levels remain difficult to achieve. Imaging the β Dr using autoradiography has been previously investigated (Rufer and Preusser, 2009; Guérin et al., 2012b; Smedley et al., 2020). However, most systems have been designed for high Dr of irradiation in medical studies and remain imprecise for natural sediment samples with low Dr, even after months of exposure.

Martin et al. (2022) developed a system dedicated to image these low Dr samples with high resolution (250 μm pixels) and high sensitivity with a quantification limit of 422 μGy per pixel that can be brought down by integrating areas of several pixels. In this previous study, the advantage of using Al_2O_3:C thin film, pulsed laser stimulation and time resolved OSL imaging was investigated. The precision of the calibration and the linearity of the dose response were determined using exposure to homogenised powder samples of known radioactivity and Monte Carlo modelling of the β and γ attenuation factors. Testing the application of the system to the real case of a heterogeneous sample is the next step for demonstrating the utility of this system and to assess what new data it can bring for the study of variations in beta Dr.

In this study, we used the system described by Martin et al. (2022) to image the β Dr of a highly heterogeneous granulite sample. Similar coarse crystalline rocks have been used for luminescence dating and thermochronology for decades (Han et al., 1999). An increasing of the interest in this type of samples started with the development of rock surface dating (Vafiadou et al., 2007). Coarse crystalline rocks usually present heterogeneous mineral distributions which can be associated with heterogeneity of β Dr. A few studies investigated the β Dr spatial

* Corresponding author. Scottish Universities Environmental Research Centre, Glasgow, United Kingdom.
E-mail address: loic.martin@glasgow.ac.uk (L. Martin).

https://doi.org/10.1016/j.radmeas.2023.107001
Received 24 November 2022; Received in revised form 17 July 2023; Accepted 2 August 2023
Available online 2 September 2023

Table 1
K, U and Th contents and associated alpha (α), beta (β) and gamma (γ) Dr in the powdered granulite reference and in the granulite chips, using the conversion factors from Cresswell et al. (2018). st.err indicates the standard errors on the mean values for the reference material; st.dev indicates the standard deviation between individual measurements.
b.Equipment and method

	K (%)	eU (ppm)	eTh (ppm)	α Dr ($Gy.ka^{-1}$)	β Dr ($Gy.ka^{-1}$)	γ Dr ($Gy.ka^{-1}$)
reference material, mean ± 2.st.err	3.46 ± 0.03	6.90 ± 0.06	16.1 ± 0.2	31.7 ± 0.2	4.41 ± 0.04	2.46 ± 0.02
10 g chips mean ± 2.st.dev	3.8 ± 1.7	7.2 ± 6.9	16.3 ± 7.2	32 ± 20	4.8 ± 2.1	2.6 ± 1.1
10 g chips minimum	3.24	3.19	10.5	20.1	3.84	1.90
10 g chips maximum	6.04	13.08	22.07	49.18	7.08	3.50

distribution in granite by associating mineral phase mapping with Dr calculation or modelling (Plachy and Sutton, 1982; Martin et al., 2018), but no direct imaging of the β Dr was done. Moreover, the frequent presence of small but highly radioactive hotspots such as zircon inclusions complicates these approaches (Fang et al., 2018). Beyond testing the autoradiography system described by Martin et al. (2022) on a real case, this study aims to investigate how accurately it is possible to image the β Dr spatial distribution in this granulite sample, how new data on β Dr distributions can lead to scattering of luminescence results from different phases and to indicate approaches with potential to improve the dating of coarse crystalline rocks.

2. Experimental

a. Samples

A granulite sample of about 30 g was selected for this study due to the high heterogeneity of this rock. Granulites are high-grade metamorphic rocks, mostly composed of feldspar and quartz. Bulk samples of this granulite and basalt chips (4 tons of each) had been procured at SUERC in 2015 to make rock boxes used to check field gamma spectrometers. The granulite source was identified by the supplier as originating from a single quarry in NE Scotland (near Elgin). Its average contents in ^{40}K, U-series and Th-series have been precisely determined using both high resolution γ spectrometry and ICPMS, conducted for preparation of a new generation of dose rate standards (Sanderson personal communication). The reference compositions of the granulite standard were determined using material which had been bulk homogenised in a concrete mixer from approximately 160 kg of material (processed in two stages with grinding in a ball mill and sieving in between the two stages of homogenisation). The reference values are derived from analysis of 10 randomly selected samples from 200 sets of material bottled from the bulk material, and were determined by ICPMS and high resolution gamma spectrometry in combination. However, because these analyses were carried on powdered and homogenised material over a considerably larger mass than the sample mass, it is difficult to compare these average contents and the corresponding β Dr with those of the 30 g sample considering the apparent heterogeneity of this granulite. In order to provide a better understanding of the variability of the contents of radioactive elements and Dr within this rock, 10 chips of about 10 g each were analysis using high-resolution gamma spectrometry: They were powdered and analysed unsealed in 50 mm diameter petri dishes using two low level shielded Ortec GMX detectors whose background rates had been determined beforehand. The standards used for calculation of activity concentrations (in $Bq.kg^{-1}$) and equivalent concentrations of K, eU, and eTh (which are series weighted averages of all the lines in the U and Th decay series used for the determination) were 10 g powdered granulite samples from the homogeneous bulk stock material presented in the same geometry with 10 g mass. The content of K, U, Th and the corresponding Dr in both the reference material and the chips are presented in Table 1. It is noticeable that while the values for the reference material and for the chips are compatible within their uncertainties, there is as expected a significant dispersion of the values obtained from individual chips.

An approximately 40 mm × 20 mm x 15 mm piece of the granulite sample was sliced using a water-cooled wafering saw using a 300 μm thick blade. Four successive 3 mm thick slices the size of approximately 15 mm by 20 mm were obtained (Fig. 1). The loss between each slice was approximately 350 μm–400 μm. Each slice weighed approximatively 2 g.

Thin Al_2O_3:C films from Landauer Ltd (Glenwood, IL, USA) (Endo et al., 2012) were used as phosphor for the autoradiography. Their properties are described in Martin et al. (2022). 15 mm × 15 mm pieces of film were prepared and bleached under white light, through a GG 495 nm long pass filter to cut UV wavelength and reduce charge transfer from deep traps during bleaching. The films were packed in pairs in black polyethylene 75 μm thick bags to protect them from α radiation and from light exposure. The bagged films were interspersed between the successive granulite slices as shown in Fig. 2. A blank was prepared by interposing bagged films between two 3 mm thick slices of high purity quartz glass.

In order to reduce the environmental radiation background during the exposure of the films to sample slices, they were placed in the STFC Boulby Underground Laboratory. This laboratory is built 1.1 km

Fig. 1. Photograph of a granulite slice (by Derek Hamilton, SUERC). This is not one of the slices used for autoradiography, but it represents a typical slice of the granulite used.

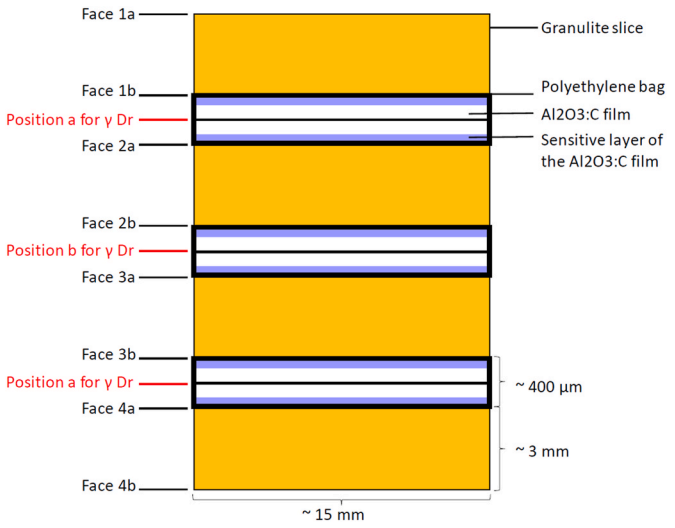

Fig. 2. Geometry of the exposure of dosimeter film to the sample slices.

underground, efficiently reducing the cosmic radiation Dr to a negligible level with a muon reduction factor of 10^6 (Murphy and Paling, 2012). The stack of slices and films was placed in a pure quartz container of 1 mm thickness to shield it from external β radiations. The samples were shielded from X-rays and γ radiation by pure copper bricks of 5 cm–10 cm thickness (Fig. 3a) and by a 20 cm thick Zeplin lead shield, which had previously been constructed for rare event physics research (Fig. 3b). The exposure time of the film was 8 months.

After exposure, the luminescence signal from each piece of film was imaged using the imaging OSL readers from Sanderson et al. (2001) and the laser pulsed stimulated luminescence protocol described in Martin et al. (2022). A 635 nm 5 mW Acculase laser from Global Laser Ltd (Abertillery, UK) was used for the stimulation, with cycles of 60 ms stimulation immediately followed by 30 ms measurement of the luminescence signal. This cycle was repeated 100 times for each point of measurement. The dark count was measured before and after each sequence of 100 cycles. In theory, the laser spot size should be < 100 µm (Martin et al., 2022). However, the effective spot size is larger because of scattering of the light at the surface of the film. We determined this effective spot size to be about 180 µm, which represents the step between pixels below the which there is partial bleaching of the next pixel. The distance between each point of measurement, which represents the resolution of the image, was chosen as 250 µm. This distance is larger than the effective laser spot size in order to ensure that there is no crosstalk between successive pixels. A 3 mm thick BG3 filter was used to protect the photomultiplier from the reflection of the laser beam and to filter part of the background photons.

Each phosphor film was bleached for at least 24 h after the first reading in order to remove the remaining signal. The remaining unbleachable background signal was measured and subtracted from the images pixel by pixel in order to take into account the variability of this residual signal, which is usually smaller than the statistical uncertainty in its measurement. The films were then irradiated by a known γ dose from a calibrated ^{60}Co source at SUERC and measured again using the same protocol in order to calibrate the exposure dose value (Martin et al., 2022). For the measurement, the phosphor films were fixed to a 10 cm by 10 cm sample holder made of an aluminium plate. This plate was polished in order the reflect the luminescence in the direction of the photomultiplier. Two reference holes in the plate fit onto pins on the scanning plate of the OSL scanning imager, allowing precise repositioning of the sample holder between successive measurements. The dark count was subtracted from the image pixel by pixel in order to correct for its variation during the time of measurement, which was about 20 h per piece of film. The blank value obtained from the average luminescence count on the blank sample was subtracted from every pixel of the images. At the end of this step, the images represent the exposure dose received during the exposure time. The uncertainty per pixel on the measured OSL signal, the background noise, the background signal and the blank are calculated by the square root of the number of photons counted. The uncertainty on the γ dose was determined to be 2.3% due to the calibration of the γ source. All these uncertainty components were added in quadrature to estimate the final uncertainty on the measured dose for each pixel.

Each side of the granulite slices was imaged by backscattered electron using a Hitachi S–3400 N Scanning Electron Microscope (SEM). The mineral corresponding to each intensity of backscattered electron signal was identified by Energy Dispersive X-Ray Analysis (EDX) using the same SEM. The mineral phase mapping of each face was then reconstructed by combining these two analyses. Four main mineral phases were identified: the quartz and albite, that are almost indistinguishable by backscattered electron imaging, represent the largest phase (72% of the analysed area), followed by the K-feldspar phase (25% of the analysed area) and the biotite phase (3% of the analysed area). The last phase regroups various heavy mineral inclusions (such as zircon or titanium oxide) and represents less than 0.1% of the analysed area.

c. Modelling and image processing

β and γ simulations of the exposure of the films protected by a 75 µm thick dark plastic bag in the granulite slice stack (composition: SiO_2 65%, Al_2O_3 20%, K_2O 12%, Na_2O 3%, density 2.6 g cm^{-3}) were conducted using the Geant4 toolkit for Monte Carlo simulation of particle to matter interactions (Agostinelli et al., 2003; Allison et al., 2016) in order to calculate β and γ attenuation coefficients due to the geometry of the exposure. This was successfully done by Martin et al. (2022). The backscattered γ contribution was not simulated because it was taken into account in the dose measured on the blank. The resulting β and γ dose attenuation coefficients for the different position of the films in the stack (Fig. 2) are presented in Table 2. Using these coefficients and the known time of exposure, each image of exposure dose was calibrated to represent the β Dr received during exposure.

Preliminary investigation by Martin et al. (2022) highlighted that the scatter of β particles in the thickness of the films and covering bag results in a convolved distribution of the β Dr recorded. In other words, the scatter of β particles in the bag and film results in blurring of the reconstructed image of the β Dr. In order to correct for this effect, a simulation was set up to calculate deconvolution parameters: two geometries were created with Geant4, respectively representing the granulite without phosphor film and the two films between two slices of granulite (Fig. 4a). β particles with the spectra of ^{40}K, U-series and Th-series were emitted from a single central radioactive column of 1 µm diameter. The β dose were imaged with a resolution of 250 µm in a 1 µm thick layer for the granulite without phosphor (representing the natural irradiation) and the sensitive layer of the films for the film exposure simulation. These images are presented in Fig. 4b for the ^{40}K β spectrum. Martin et al. (2018) have considered the extent to which the β Dr recorded in a 2D plane of a sample is representative of the β Dr in 3D in the sample, if the area of measurement or simulation is large enough to be representative of the sample and if the sample is roughly isotropic. Assuming it is the case in this study, the results from the simulation of the natural exposure can be regarded as representative of the natural scatter of the β Dr in the granulite, i.e. the natural image of the β Dr, designated as F. In the same way, the results of film exposure simulation represent the β Dr with the additional scatter from the bag and detector, i.e. the convolved images the β Dr, designated as H. The natural images F and their corresponding convolved images H are linked in the Fourier Space by equation $H = F.g$, where g is the convolution function. This convolution functions for the geometries b and c and for each β spectrum were retrieved by dividing the natural image F by the corresponding convolved image H in the Fourier Space. The difference between the

a – sample inside the copper brick shield

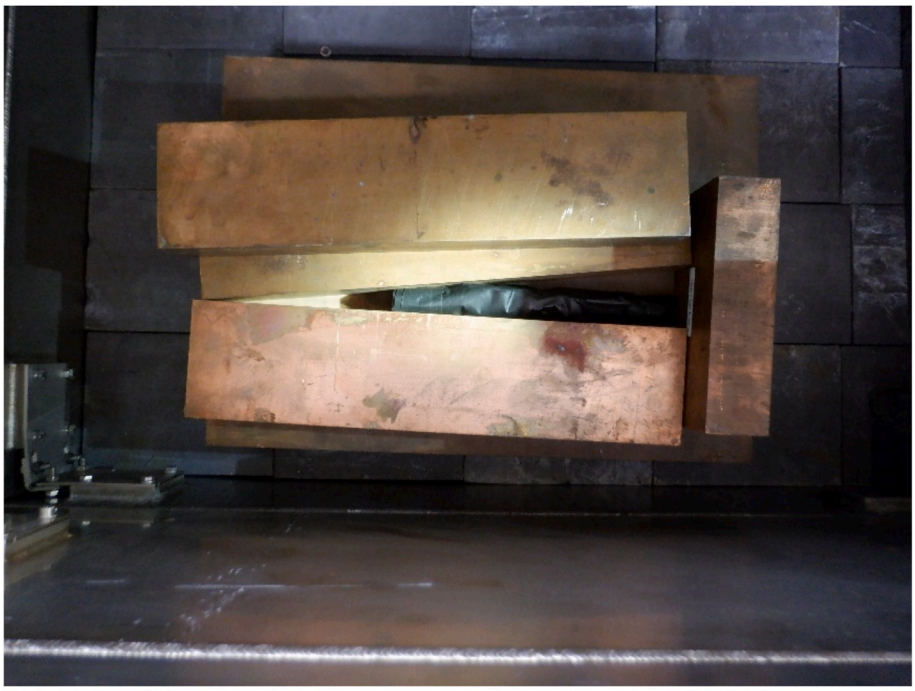

b - Zeplin lead shield used to shield the environmental γ Dr

Fig. 3. Photographs of the environmental radiation shielding materials. a – sample inside the copper brick shield. b - Zeplin lead shield used to shield the environmental γ Dr.

convolved and deconvolved images, as well as the additional scatter that the convolution function represents, can be visualised by the transects of their spatial distributions for the ^{40}K β spectrum on Fig. 5.

The image of the natural scatter of β Dr is on the left, the image of the β Dr scatter during film exposure is on the right.

In theory, the inverse process can be applied to reconstruct the deconvolved image F' of the β Dr in the granulite by dividing the convolved image H, obtained by autoradiography after calibration, by the convolution function g. However, this process is extremely sensitive to noise and statistical scattering that are common with OSL measurements and would only lead to incoherent images if directly applied. In order to minimize the influence of noise and statistical scattering, a deconvolution algorithm must be employed. We used the Richardson-Lucy algorithm (Richardson, 1972) with the convolution function

Table 2
Dose rate attenuation factors for the irradiation of Al_2O_3 films calculated from simulations. *The attenuation factors are defined as the fraction of dose rate received by the film over the corresponding infinite matrix dose rate.*

Dr component	^{40}K	U-series	Th-series	Average value[a]
β Dr attenuation factor	64%	60%	55%	62 ± 3%
γ Dr attenuation factor at a[b]	5.2%	6.2%	5.7%	5.6 ± 0.4%
γ Dr attenuation factor at b[b]	5.5%	6.6%	6.0%	6.0 ± 0.4%

[a] Average coefficient values are calculated by weighting each component by the average proportion of β or γ dose rate that it represents. The uncertainty indicated is the standard deviation between the coefficients for the different components weighted by their dose rate contribution.
[b] a and b refer to the position for γ Dr on Fig. 2.

obtained in the previous step for reconstructing the images of the β Dr distribution images from the autoradiography of the different slices. The calculations were done with the ImageJ software (Rasband, 2012; Schneider et al., 2012) using the DeconvolutionLab2 package (Sage et al., 2017). This algorithm has been successfully used for deconvolution of autoradiography in medical studies (Zhang et al., 2008). The difference between the initial convolved autoradiography images and the resulting deconvolved β Dr images is illustrated on Fig. 6 using the convolution function calculated from simulations and compared to the mineral phase image. It is noticeable that the deconvolution increases the sharpness of the β dose rate images and improves the match between dose rate boundaries and the mineral phase maps.

The position of the dosimeter film against the granulite slice during exposure is indicated by the yellow square on the mineral mapping. The Dr values correspond to the dose received by the different pixels during the exposure to the sample.

The mineral phase mapping of each slice was superimposed to the corresponding image of β Dr. The rotation and translation necessary to this superimposition were done by adjusting the shape and centroid of recognizable features, such as the highly radioactive K-feldspar areas.

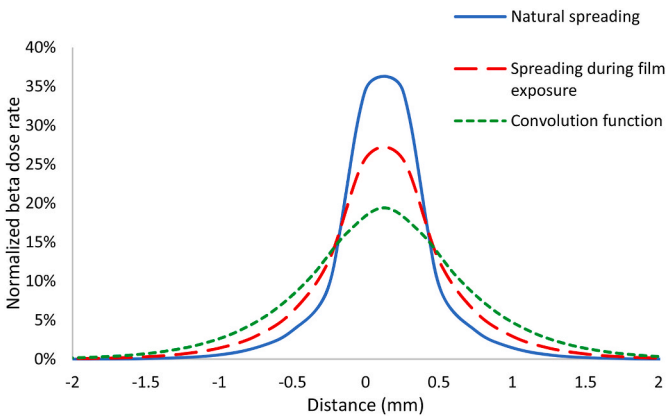

Fig. 5. Transect of the β dose natural and convolved image and of the spatial distribution of the convolution function obtained from Monte Carlo simulation.

Using the different mineral phases as regions of interest of the β Dr images, the average value and the histogram of the distribution of the β Dr were obtained for each mineral phase. As the heavy mineral inclusion phase and the biotite phase represent only a small fraction of the analysed surface, the results for these phases cannot be considered as representative. Consequently, these results are not presented and the further analyses focused on the K-feldspar phase and the quartz and albite phase.

3. Results

Fig. 7Associates the different β Dr images obtained with the mineral phase maps of the corresponding slice of granulite. The resolutions are 250 μm and 20 μm respectively for the β Dr images and for the mineral mappings. The number of counts C corresponding to the beta dose rate is calculated according to formula (1):

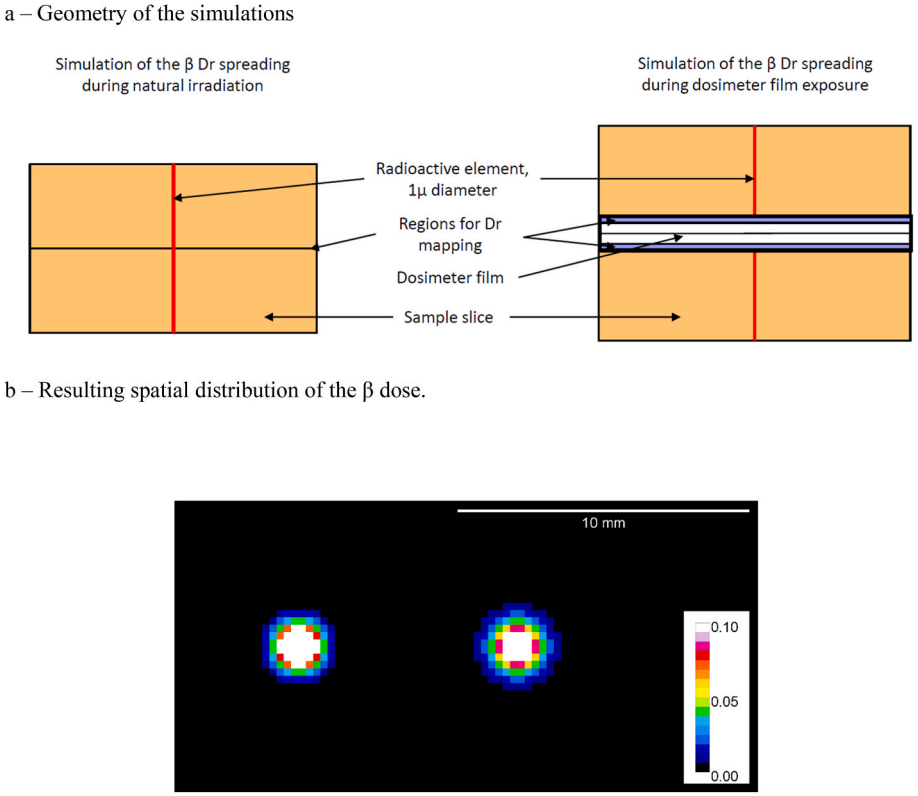

Fig. 4. Simulation of β particles scatter during exposure. a – Geometry of the simulations. b – Resulting spatial distribution of the β dose.

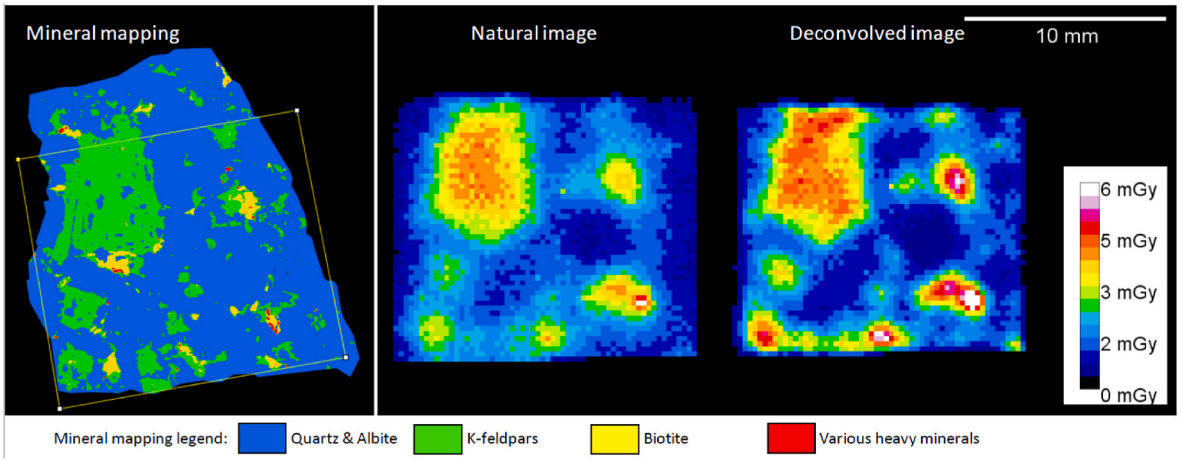

Fig. 6. Effect of the deconvolution on a β Dr image.

$$C = C_{raw} - C_{blank} - C_{dark} \quad (1)$$

With C_{raw} being the raw number of counts measured on a Region of Interest (ROI), C_{blank} being the number of counts for the same ROI on the blank image (after subtraction of the dark counts on this image) and C_{dark} being the number of counts of the dark counts measured during the same cycle than the raw image.

All the uncertainties are given as twice the standard deviation. st. dev, the standard deviation on the number of counts for the beta dose rate over a given ROI, $st.dev_c$, is calculated by the quadratic sum of the standard deviation of the different contributions:

$$st.dev_c = \sqrt{(st.dev_{raw}^2 + st.dev_{blank}^2 + st.dev_{dark}^2)} \quad (2)$$

With $st.dev_{raw}$ being the standard deviation over the raw count number, calculated as the square root of the total counts over the ROI:

$$st.dev_{raw} = \sqrt{(C_{raw})} \quad (3)$$

$st.dev_{blank}$ represents the standard deviation over the blank count over the ROI, calculated as the quadratic sum of the square root of the counts and the standard deviation over the dark count of the blank image $st.dev_{dark\ blank}$:

$$st.dev_{bank} = \sqrt{\left(\left(\sqrt{(C_{blank})}\right)^2 + st.dev_{dark\ blank}^2\right)} \quad (4)$$

The standard deviations of the dark counts $st.dev_{dark}$ and $st.dev_{dark\ blank}$, which follow a Poisson law, are determined by:

$$st.dev_{dark} = st.dev_{dark\ pixel} \Big/ \sqrt{N} \quad (5)$$

with $st.dev_{dark\ pixel}$ being the standard deviation between the dark counts measured for every pixels of the ROI and N being the number of pixels in the ROI.

The dose of radiation D received by the film during exposure is calculated as:

$$D = C.D_{calib}/C_{calib} \quad (6)$$

with D_{calib} being the known γ dose delivered during calibration and C_{calib} the number of counts measured on the calibration image using Equation (1). The uncertainty σ_D on D is determined by:

$$\sigma_D = D.\sqrt{(st.dev_c^2 + \sigma_{D\ calib}^2 + st.dev_{calib}^2)} \quad (7)$$

with $\sigma_{D\ calib}$ being the uncertainty on D and $st.dev_{calib}$ the standard deviation over the counts on the calibration image, calculated according to Equation (2).

The corresponding β dose rate Dr is determined by the equation:

$$Dr = D.F_\beta.F_\gamma/T \quad (8)$$

with F_β being the attenuation factor for β dose rate resulting due to the attenuation within the phosphor film, F_γ being the attenuation factor for removing the γ dose rate contribution and T being the time of exposition of the phosphor film to the sample. The uncertainty σ_{Dr} on Dr is determined by:

$$\sigma_{Dr} = Dr.\sqrt{(\sigma_D^2 + \sigma_{F\beta}^2 + \sigma_{F\gamma}^2 + \sigma_T)} \quad (9)$$

with $\sigma_{F\beta}$, $\sigma_{F\gamma}$ and σ_T being the uncertainties on F_β, F_γ and T respectively.

Per pixel, the average counts from the OSL signal originating from the β Dr contribution and from the γ Dr contribution are respectively 542 ± 50 and 26 ± 1. The average dark count of the photomultiplier is 90 ± 14 per pixel and the average residual signal is 320 ± 24 per pixel. The average count on the blank, once the dark count and residual count are subtracted, is 22 ± 31. This corresponds to a Dr received by the blank of 0.10 ± 0.14 $Gy.ka^{-1}$ per pixel, or 0.10 ± 0.05 $Gy.ka^{-1}$ average over the whole image. The pixel values from beyond the boundaries of the slices, identified using the SEM mapping (Fig. 7), have not been used in the subsequent analysis.

The mineral mappings are on the left and the Dr images on the right. The position of the dosimeter film against the granulite slice during exposure is indicated by the yellow square on the mineral mapping.

The average β Dr measured for each slice as well as the mean value is presented in Table 3. We can observe that although the mean β Dr value from autoradiography is higher than the value from the powdered reference material, it is well within the variability of the mean β Dr measured from the chips (Table 1). Considering the proximity of the total mass represented by the slices used for autoradiography (8 g) with the average mass of the chips (10 g), we can conclude that the mean β Dr determined by autoradiography is compatible with the measurements by high resolution γ spectrometry. The variability of the β Dr measured by autoradiography of the different slices (weighting approximatively 2 g each), as well as the standard deviation between pixel for each image, allow appreciating the variability of the β Dr at these smaller scales. The significant increase of the standard deviation between pixels for face 3 b and 4a is noticeable: it corresponds to the presence of a high radioactivity hotspot where the highest dose rate of these mapping, Dr 199 ± 9 $Gy.ka^{-1}$, was measured.

β Dr distributions for the K-feldspar phase and the quartz and albite phase from different dose rate images are compared on Fig. 8a and Fig. 8b, as well as the average β Dr distribution for each of these phases on Fig. 8c-d. A logarithmic scale is used in Fig. 8d in order to display the high Dr contribution from the different hotspots visible on Fig. 7.

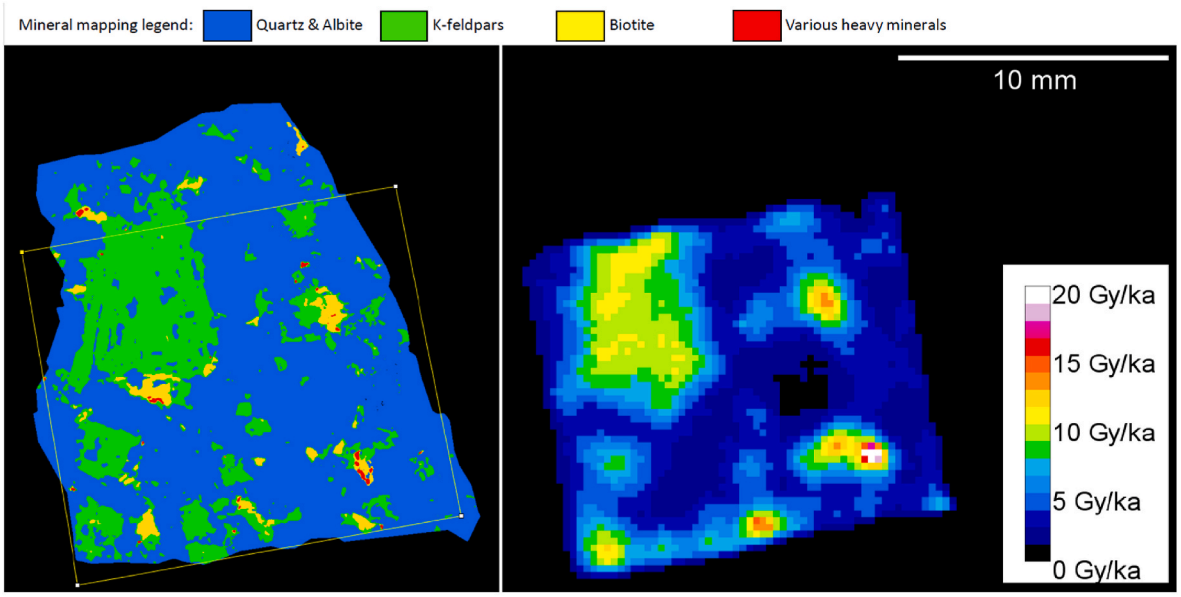

b – Face 2a

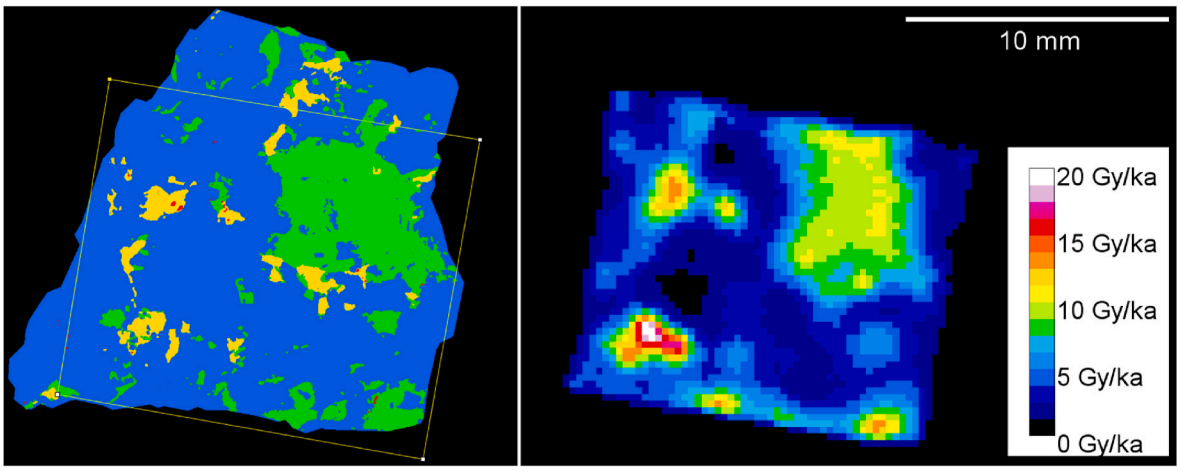

c – Face 2b

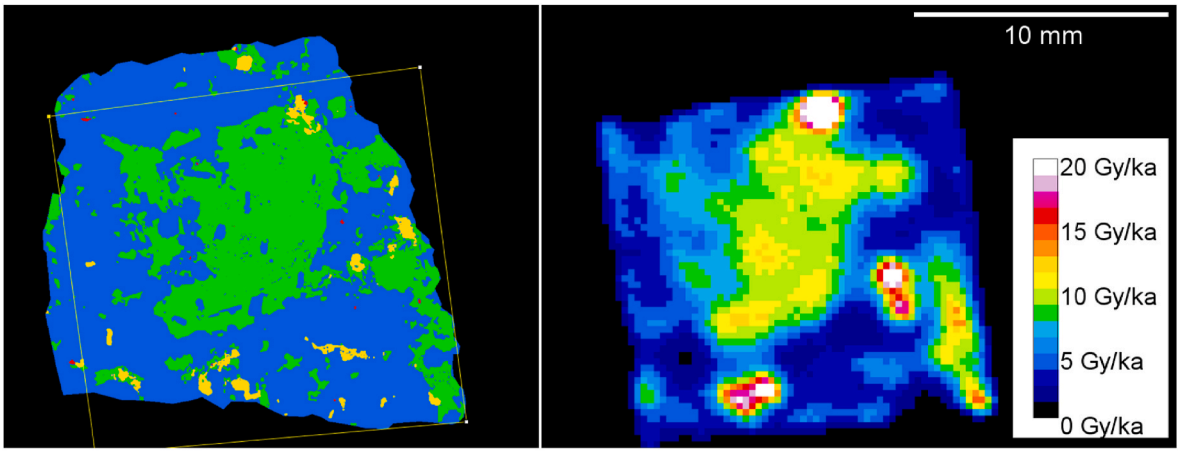

d – Face 3a

Fig. 7. β Dr images associated with the associated mineral phase mappings.

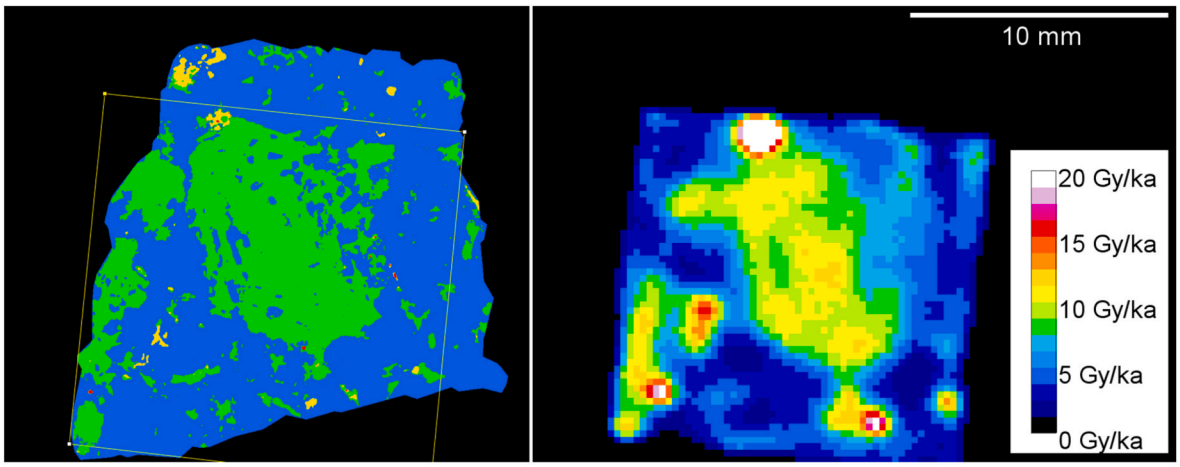

e – Face 3b

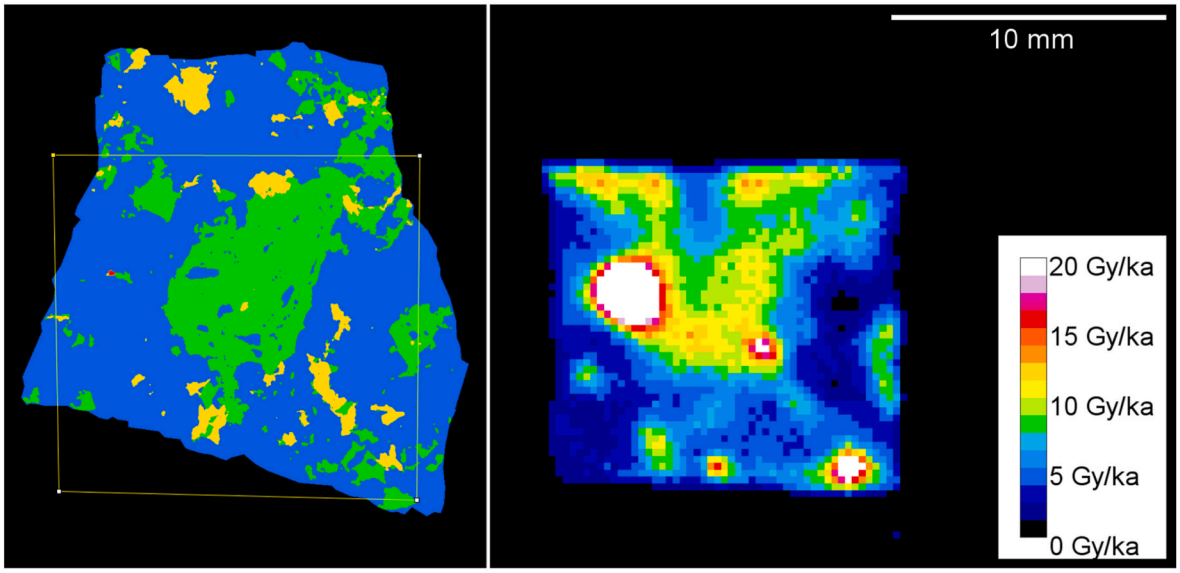

f – Face 4a

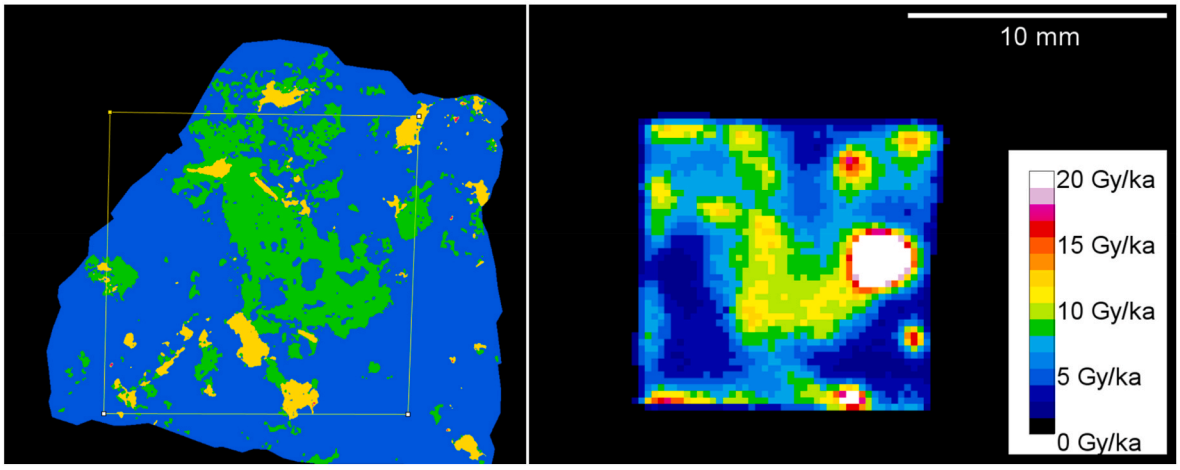

Fig. 7. (*continued*).

Table 3
Variation of β Dr measured by autoradiography of the different slices. 2σ is twice the standard deviation of the β Dr between the pixels and twice the standard deviation respectively for the individual images and for the average value. The uncertainties provided with the mean β Dr are the uncertainty over the measurement of the corresponding integrated area as defined at the beginning of part 3.

Image	Face 1 b	Face 2a	Face 2 b	Face 3a	Face 3 b	Face 4a	Average
Mean β Dr (Gy.ka^{-1})	4.8 ± 0.3	5.1 ± 0.3	6.6 ± 0.3	6.9 ± 0.3	7.8 ± 0.4	8.5 ± 0.4	6.5 ± 0.3
2.St.dev (Gy.ka^{-1})	5.7	6.1	8.4	8.5	18.4	26.5	3.3

4. Discussion

a. Validity of the calibration

The accuracy of the calibration method employed was demonstrated for homogeneous materials in Martin et al. (2022) and there is no evidence to suggest additional systematic errors in the calibration used to study the heterogeneous forms within this study, even if this cannot be completely ruled out without additional measurements of the radioactivity of the slices. The only difference with the protocol of Martin et al. (2022) is the deconvolution step, which does not modify significantly the average Dr value. The effect of heterogeneity of the sample could have a significant influence if the luminescence sensitivity of the phosphor film was highly variable pixel to pixel, which is not the case with no significant variation of the sensitivity observed beyond the uncertainty of the counting statistic. The average β Dr of 6.5 ± 0.3 Gy.ka^{-1} (this uncertainty is the uncertainty of the measurement, representing the precision of measurement for a sub-sample of ~8 g) calculated over the slices (Table 3), representing approximately 8 g of material, is compatible with the average value of 4.8 ± 2.1 Gy.ka^{-1} (this uncertainty is twice the standard deviation between the values for the different chip, characterizing the variability between sub-sampling of ~10 g) measured by high-resolution gamma spectrometry on the 10 g chip within the uncertainty related to the chip-to-chip variability of radioactive elements (Table 1). This result also supports the validity of the calibration method used here to determine the dose rates distributions from these heterogeneous rock slices.

Considering this higher radioactivity of the slices (Table 3), compared to the radioactivity of the powdered reference sample (Table 1), the γ Dr contribution, calculated using the Dr values from Table 1 and the coefficient from Table 2, may be underestimated for this sample of granulite which seems more radioactive than the homogenised powder produced from a considerably larger quantity of material. However, as this contribution represents less than 1% of the average Dr, this has no significant effect on the average β Dr calculated nor its distribution and doesn't affect the observations presented in this study. A more accurate γ contribution could be calculated using the radionuclide contents of the different slices, which would require further measurements.

The significant difference between the radioactivity of this sample and the average value for this granulite, as well as between the different 10 g chips, raises the question of the representativeness of this sample: are the measured β Dr and its distribution representative of the those that would affect an OSL sample of this granulite? There are two scenarios possible here: either the OSL signal is measured on the same sample that is used for Dr imaging, or it is measured in another sample of the same granulite. In the first case, as the sample is of a similar size as the typical sample measured for OSL dating, the Dr distribution observed can be considered representative of the Dr received in the grains for OSL measurement. OSL imaging could also be used directly on the slice in order to record the spatial distribution of the OSL signal, that could be directly compared to the β Dr spatial distribution. With the recent development of OSL imaging, in particular for rock surface dating (Sellwood et al., 2022), it is likely that this approach will be developed further in a near future. In the second case in the which the sample for OSL and the sample for autoradiography are not the same, neither the OSL sample alone nor the β Dr distribution can be considered representative of the whole sample, considering its high heterogeneity. Each represents the local characteristics of the sample, and only the multiplication of measurements on several samples from the same material, or the analysis of a larger area or mass of material, could provide information that could be considered as representative of the whole material. The representativity of both the sample for autoradiography and the sample for luminescence measurement should be addressed through quantitative method in order to assess the accuracy of the dating (Ingamells, 1974). The autoradiography method used for this study offers the possibility of analysing large sample areas, up to 10 cm by 10 cm. β Dr imaging of large areas will be investigated in order to assess the advantages of this approach.

b. Precision of the measurements

The uncertainty of the β Dr per 250 μm pixel ranges from 30% to 4.4% for respectively the lowest Dr of 1.7 ± 0.5 Gy.ka^{-1} and the highest Dr 199 ± 9 Gy.ka^{-1}, with an average uncertainty of 10% on the average Dr value per pixel of 6.5 ± 0.6 Gy.ka^{-1}. The average blank Dr per pixel is 0.10 ± 0.14 Gy.ka $^{-1}$, which correspond to an average blank value of 0.10 ± 0.05 Gy.ka $^{-1}$ over an approximative 15 mm by 15 mm image, while Martin et al. (2022) measured a blank of 0.23 ± 0.08 Gy.ka $^{-1}$ for a similar area without underground exposure. While these values are technically compatible within the limit of their uncertainty, the probability of it is low and it seems more likely that the underground exposure decreased the environmental background, improving the precision of the β Dr images. Further analyses are required to confirm this. A reduction of the dark count of the photomultiplier and of the residual signal of the film would also enable more precise determination of the blank Dr and improve the precision of the measurement, in particular for the lowest Dr.

The precision on the measurement of high Dr tends to a limit of about 4.3%, which corresponds to the combination of the uncertainty on the calibration of the γ source used for the calibration (2.3%) and of the uncertainty on the β Dr attenuation factor (3.7%). Improving the precision of the γ source calibration would slightly improve the precision of the results. The uncertainty on the attenuation factor is related to the difference of β absorption between the ^{40}K, the U-series and the Th-series contribution is more complex to reduce. Finding a geometry of exposure that minimize this difference is a possibility that will be investigated. It is noticeable that a significant decrease of this uncertainty is expected for samples where the β Dr is dominated by one of the contributions.

The precision of the β Dr images obtained in this study represents the best for autoradiography of natural mineral sample published so far (Rufer and Preusser, 2009; Guérin et al., 2012b; Smedley et al., 2020). This precision seems also better than the precision of Timepix detectors (Romanyukha et al., 2017), although the comparison is not as straightforward. Fu et al. (2022) obtained with a Timepix a precision of about 31% for a β Dr of 3.4 Gy ka^{-1} with a resolution of 220 μm. The precision of the autoradiography system presented in this study for a similar Dr is about 15%. However, the precision of lower Dr is limited by the significant residual signal and will be over 100% for Dr lower than 0.5 Gy.ka^{-1}, similarly to that obtained by Fu et al. (2022). It seems that the autoradiography system gives similar results to the protocol developed by Fu et al. (2022) for low Dr, but better results for Dr greater than 1 Gy.ka^{-1}. If the residual signal of the alumina film could be lowered, the precision of the autoradiography system for low Dr would

a – β Dr distribution in the K-feldspar phase from each image

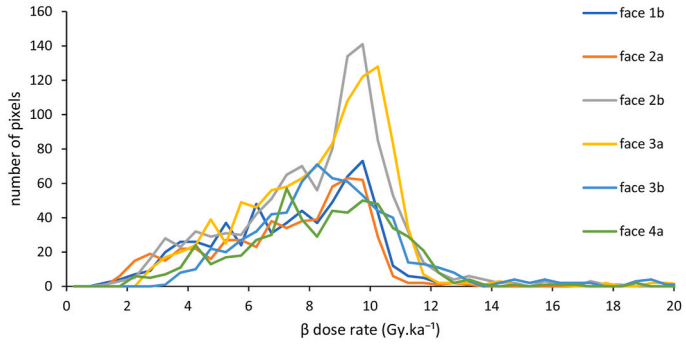

b – β Dr distribution in the quartz and albite phase from each image

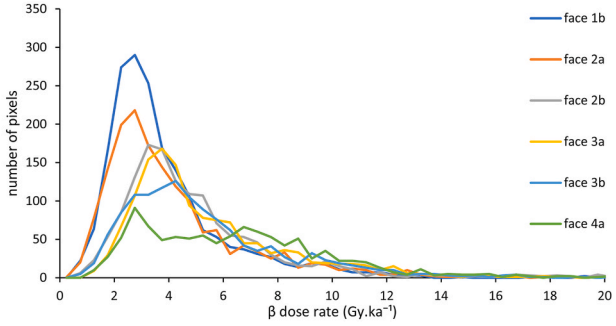

c – β average Dr distribution between all the images

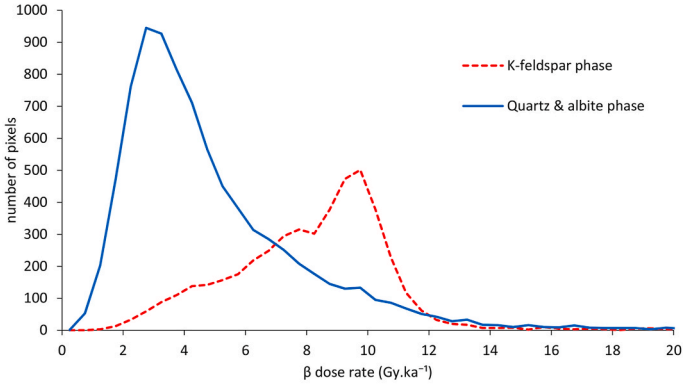

d - β average Dr distribution between all the images, logarithmic scales

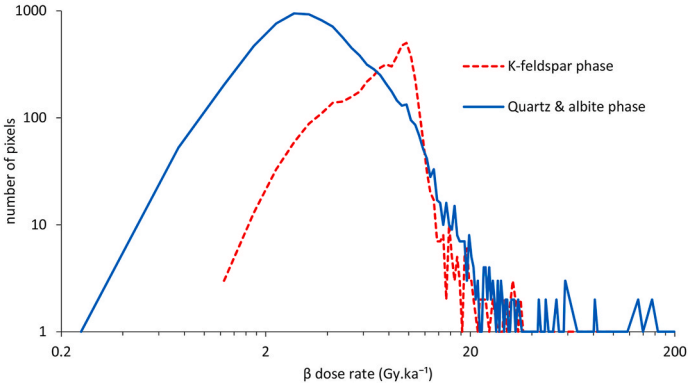

Fig. 8. β Dr distribution of the different mineral phases a – β Dr distribution in the K-feldspar phase from each image. b – β Dr distribution in the quartz and albite phase from each image. c – β average Dr distribution between all the images. d - β average Dr distribution between all the images, logarithmic scales.

significantly increase. Processes to bleach this signal are being investigated.

Another important point of comparison with the Timepix system is the time of analysis. The determination of the Dr images recorded by a 10 mm by 10 mm area of film (which is approximatively the size of a Timepix sensor) with the OSL scanner would take approximately 5 days, which includes the 3 scans necessary, the bleaching time and the irradiation time. However, it would also require several months of exposure of the film to the sample prior to the measurement (8 months in the case of this study). The Timepix measurement took only 10–28 days for Fu et al. (2022) and increasing the counting time would lead to an increased precision that could match the autoradiography one. However, this needs to be put into perspective of studies implying multiple samples, which is usually the case in OSL dating: Timepix systems can only analyse one sample at a time and with a limited area of analysis, while multiple samples can be exposed to the alumina film for autoradiography at the same time and larger area (up to 10 cm by 10 cm) can be measured with the OSL scanner. It is also possible to reduce the time of analysis of multiple samples by alternating the samples for reading, bleaching and γ irradiation (for example, by scanning a sample while another is being bleached and another irradiated). This possibility of processing multiple samples in parallel as well as large samples represents an advantage of the autoradiography method which would be very convenient in study involving as rock surface dating, for the which such samples are frequent.

c. Robustness of the positioning

There was no visible shift between the images of corresponding to the measurement of the signal from exposure, of the blank and of the calibration dose. This indicates that the repositioning of the sample fixed on the sample holder on the scanning plate is accurate at less than the image resolution of 250 μm.

The accuracy of the superposition of Dr images with the corresponding mineral phase mappings using recognizable features can be discussed. It is relatively easy to implement for some Dr images where some features are easy to recognize (Fig. 7a) but can be more difficult for more complex images such as Fig. 7e which is affected by the presence of a strong radioactive hotspot. It is noticeable that a shift of the superpositioning by one- or two-pixels size (250 μm–500 μm) does not significantly affect the global shape of the Dr distribution nor the average β Dr calculated for the different phases, except for Fig. 7c-d because of the presence of the strong radioactive hotspot between the K-feldspar phase and the quartz & albite phase. Therefore, this method for superimposing Dr image with phase mapping cannot be considered as robust in the presence of strong hotspot and should be replaced by a better one. Fu et al. (2022) used an α source handed above the sample and the Timepix detector in order to record the shape of the sample before imaging the β Dr. A similar method could be investigated with the phosphor film, but the α-thick black bag used to encapsulate the film limit this possibility. The use of a support that will hold in place both films and samples with a position reference seems a more practical solution that is currently under investigation. Another possibility to improve the superposition of Dr images with mineral mapping would be to increase the size of the piece of film to image a larger area of sample, as more distant recognizable features would enable a more precise alignment.

d. Effect of the scatter of β particle in the detector

Figs. 4 and 5 demonstrate the need for deconvolution in β Dr imaging or for other data processing method in order to take into account the scatter of β particles within the detector thickness. This step significantly improves the accuracy of β Dr imaging and is necessary to evaluate in which extent it can affect individual grains and the scattering of luminescence result. It seems that the effect of β particles scattering within the detector on Dr imaging has been overlooked so far. It is noticeable that this effect is significant in this study despite of a relatively small detector thickness (Fig. 2). Other autoradiography plates or the sensitive part of Timepix detectors can be significantly thicker, sometime more than 1 mm. A wider scattering of the β particles and a stronger blurring of the β Dr images can be expected in those detectors compared to the films used for this study. Consequently, it is possible that previous studies have underestimated the scattering of the β Dr in the samples investigated. Monte Carlo simulations of this effect followed by a deconvolution seems an appropriate method to take it into account and gave visible results in this study. Direct measurements and further Dr modellings will be investigated in order to confirm these results.

e. β Dr determination in the different mineral phases

Average β Dr of 5.55 ± 0.24 Gy.ka^{-1} and 8.42 ± 0.36 Gy.ka^{-1} are measured using the β Dr images for respectively the quartz-albite phase and the K-feldspar phase. The precision on these values is limited by the 4.3% uncertainty relative to the uncertainty on the calibration of the γ source and on the β Dr attenuation factor.

The standard β Dr calculation method for OSL dating is based on the inclusion method which consist of applying an attenuation factor for grain size to the average bulk β Dr as well as a self-dose factor to the internal β Dr for the K-feldspar (Fleming, 1970; Mejdahl, 1983). This method was initially developed for thermoluminescence dating of ceramics. The Dr is calculated considering the hypothesis of a small number of datable grains inside a homogeneous matrix. These grains are assumed spherical and to be far enough from other grains to have no effect on their Dr, i.e. there is no grain-to-grain irradiation or lower Dr due to the presence of nearby low radioactivity grains. This model is widely applied in luminescence dating including of coarse crystalline rocks (King et al., 2016; Stalder et al., 2022), even if these samples may not fit in the dosimetric hypothesis of the inclusion model. It is important to remember that the paleodosimetric community has long been aware of the difficulty of calculating Dr in coarse crystalline rocks and, if possible, prefers fine crystalline rocks (Sanderson et al., 1988). Some attempts have been made for developing models more adapted to coarse crystalline rocks but their use remains marginal (Plachy and Sutton, 1982; Martin et al., 2018; Semikolennykh et al., 2022), maybe because they require more analysis than is commonly applied in luminescence dating and often lack of strong experimental validation.

We calculated the β Dr of the K-felspar phase and of the quartz & albite phase using the inclusion Dr model in order to compare them with those obtained by autoradiography. We considered the average β Dr measured by autoradiography (6.5 ± 0.3 Gy.ka^{-1}), 250 μm grains and the attenuation and self-dose factors from Guérin et al. (2012a). β Dr of 5.92 ± 25 Gy.ka^{-1} and 6.95 ± 0.25 Gy.ka^{-1} were obtained for respectively the quartz-albite grains and the K-feldspar grains, including an internal β Dr contribution in the later corresponding to a K content of 14%.

If the values for the quartz and albite phase from the autoradiography and from the standard calculation (5.55 ± 0.24 Gy.ka^{-1} and of 5.92 ± 0.25 Gy.ka^{-1} respectively) are compatible within the uncertainty there is a significant difference of about 20% between the Dr calculated for the K-feldspar phase from the autoradiography and from the standard calculation (8.42 ± 0.36 Gy.ka^{-1} and 6.95 ± 0.25 Gy.ka^{-1} respectively). This highlights the impact on β Dr of K-feldspar grain clustering in sample, such as it can be for various coarse crystalline rocks. Even for the quartz and albite phase, despite of the fact that the two methods give compatible results, the validity of the standard model should be questioned as it does not seem to correspond to a physical reality in such heterogeneous samples. The actual attenuation and self-dose factors should be related to the size and shape of the grain clusters, such it has be investigated in King et al. (2016), Rades et al. (2018), Jenkins et al. (2018), Cunningham et al. (2022) and Semikolennykh et al. (2022). However, as these shapes are usually highly irregular while

most software and stereological correction assume a spherical shape. Considering that the size of the grain clusters is often larger than the average β particle range of 2 mm in rocks, their irregular shapes must have an impact on the internal β Dr. It is also noticeable that in Rades et al. (2018), Jenkins et al. (2018), Semikolennykh et al. (2022), the authors used the apparent size of the clusters on the image as real size while it is in reality the size of the interception of the clusters by the slicing. This may induce a significant error in the estimation of the size distribution of the clusters, which could have been corrected using stereological corrections (Martin et al., 2015; Bailiff, 2018). However, it is necessary to analyse an area large enough to be representative of the size distribution of the clusters in the sample for these corrections to be accurate, which is probably not the case in those study nor in this one. Simulation of the β Dr (Martin et al., 2018) or direct measurement such as those presented in this study seem to be more accurate and promising solutions.

f. Effect of the β Dr distribution on the luminescence measurements

The standard deviation calculated on the β Dr distributions (Fig. 8) are 35% and 87%, respectively for the K-feldspar phase and the quartz and albite phase. The extreme scattering obtained for the quartz and albite phase is mostly due to the influence of a few strong radioactive hotspots (Fig. 7). The standard deviation for this mineral phase below the threshold of 10 Gy.ka^{-1} (which corresponds to the Dr peak of the K-feldspar and excludes the Dr from the hotspots) is only 41%, which is comparable to the K-feldspar one. The standard deviation of the Dr in the K-feldspar phase is less influenced by the hotspot because its Dr is higher in average and because the hotspots are generally closer to the quartz and albite phase than to the K-feldspars phase. Smedley et al. (2020) and Fu et al. (2022) obtained slightly lower scattering values for heterogeneous samples of different natures, but with the same order of magnitude.

The effect of these wide β Dr distribution to the scattering of luminescence measurements can be reconstructed through a random sampling of n values within it, in order to represent the Dr in aliquot constituted from n grains from the crushed sample. For representing the total Dr, the average α and γ Dr calculated from the average radionuclide contents (Table 1) were added as an offset to the β Dr distributions, as well as the standard value of the cosmic Dr at sea level of 0.3 Gy.ka^{-1}. α efficiency factors of 0.03 and 0.09 were applied to the respective α Dr contribution to the quartz grains (assuming that the β Dr distribution in quartz grain is similar than in the quartz and albite phase) and to the K-feldspar grains in order to consider its lower efficiency to produce luminescence compared to the other Dr contribution. The total Dr offsets from these contributions represent 3.71 ± 0.02 Gy.ka^{-1} and 5.61 ± 0.03 Gy.ka^{-1}. The likely heterogeneity of the α Dr is not considered here, therefore the results represent only the share of scattering of the total Dr due to the β Dr heterogeneity. The standard deviations of Dr received between these virtual aliquots were calculated using Monte Carlo sampling in the total Dr distribution, for different size of aliquots. The results, presented on Fig. 9, follow perfectly a rule of $STD_n = STD_1/\sqrt{(n)}$, Where STD_n is the standard deviation between Dr received by aliquots of n luminescent grains and STD_1 the standard deviation between Dr of single luminescent grains. The distinction between the number of grains per aliquot and the number of luminescent grains per aliquot is important, because usually only a small fraction of quartz grains is luminescent while the proportion of luminescent K-feldspar grains is significantly larger (Duller et al., 2003; Smedley et al., 2019). It is also important to remember that the calculated scatterings are resulting only from the β Dr spatial distribution, and do not consider the scattering due to α Dr spatial distribution, to partial bleaching or to variation of the luminescence efficiency between grains. The Dr scattering of K-feldspars, while significant at the single grain scale, quickly decreases with the aliquot size, and is reduced to a few percent above n = 100 luminescent grains per aliquot. The Dr scattering for the quartz and albite aliquot is significantly larger, and still about 9% for aliquots with 100 luminescent grains. However, like previously explained, only a small fraction of the quartz grains is sensitive to luminescence; as a result, the scattering of luminescence signal between quartz aliquots of about 100 grains would probably be around the results for 1 to 10 luminescent grains, which would give a scattering due to the β Dr spatial distribution ranging from about 87% to 27%.

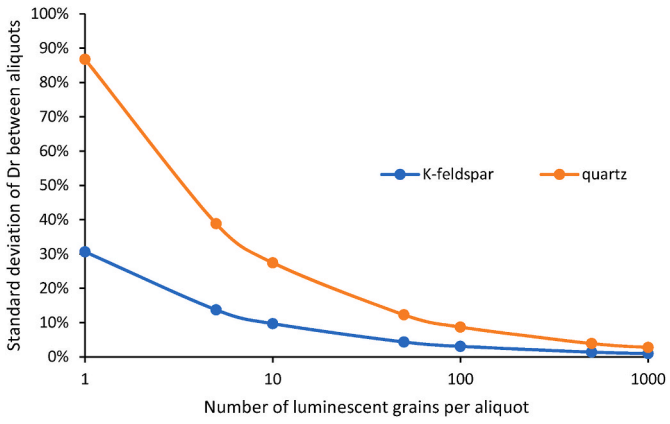

Fig. 9. Scattering of the Dr received by aliquot due to the β Dr heterogeneity depending on the number of luminescence grains per aliquot.

The variation of luminescence sensitivity between grains also exists within K-feldspar, even if it is usually not as strong as for quartz grains (Duller et al., 2003; Smedley et al., 2019). In order to calculate a more accurate estimation of the scattering between aliquots, the distribution of luminescence sensitivity should also be integrated to the calculation. This distribution could be obtained using single grain OSL, or OSL scanning on sample slice using for example the same scanner as for the autoradiography, with a set of optical filters adapted to the luminescence signal of the grains. This second option would allow to compare directly the spatial distribution of β Dr and of luminescence sensitivity, which could considerably improve the precision and accuracy of the dating for similar sample by taking into account the scattering due to these two phenomena. In the same way, adding to the analysis the spatial distribution of the α Dr and of the α efficiency for luminescence should improve the accuracy of the analysis. While it is technically feasible using autoradiography, laser ablation ICPMS or fission track mapping, the setup of such experiment is much more complex or more expensive than for the β Dr.

5. Conclusions

The autoradiography system used for this study allowed measuring the most precise β Dr images so far achieved of a natural mineral sample with a resolution of 250 μm. This is thanks to the combination of high sensitivity Al_2O_3:C film, ultra-low background underground exposure, laser pulsed-stimulated OSL scanning and Monte Carlo simulations of β particle scattering. The advantage of lower background provided by underground exposure needs to be investigated further. Improvement of the method of superposing the Dr image with mineral phase mapping are being investigated in order to guarantee the accuracy of the Dr distribution observed. The reduction of the residual signal would also significantly improve the precision of the measurement, especially for low radioactivity samples; Improving the precision on the calibration will benefit to the measurement but more particularly to the higher Dr values.

The β Dr value in the different mineral phases of the sample can be significantly affected by the clustering of grains of the same mineral, which make the standard method of calculation irrelevant for the K-feldspar grains this case. Significant error on the Dr determination and on the age calculation can be made if this effect is not considered.

Methods of Dr determination considering the size and shape of the grain cluster, which include β Dr imaging, should be considered for similar coarse crystalline rocks in order to avoid this bias.

Scatter in the beta Dr of 35% and 87% for the K-feldspar phase and for the quartz and albite phase respectively were observed. The high value of the scattering in the quartz and albite phase results from the influence of a few highly radioactive hotspots. Identifying these hotspots and their proximity to the different mineral phases seems necessary for evaluating the potential scattering of luminescence resulting from their influence. β Dr imaging is a useful tool to do so. While the influence of β Dr scattering on luminescence results should be significantly decreased when using multi-grains aliquot for the K-feldspar, it is likely to be still significant for multi-grains aliquots of quartz because of the stronger influence of the hotspots and because only a small proportion of quartz grains are luminescent. The determination of the proportion of scattering of luminescence results coming from β Dr heterogeneity can improve the precision of luminescence dating by reducing the deviation between results.

The high sensitivity β Dr imaging system presented in this study offers great prospect for taking into account the β Dr spatial distributions of heterogeneous samples such as coarse crystalline rocks. In particular, the possibility of imaging large sample area up to 10 cm by 10 cm should offer a significant increase of the accuracy of such analysis and will be investigated. Comparison of β Dr imaging with OSL imaging would allow directly taking into account their spatial variations, which should considerably improve the accuracy of the dating of heterogeneous samples. This offer many prospects of application of this method to dating cases of coarse crystalline rocks and other heterogeneous samples, in particular for rock surface dating for the which OSL imaging is frequently used.

Declaration of competing interest

The authors declare that they have no known competing financial interests or personal relationships that could have appeared to influence the work reported in this paper.

Data availability

Data will be made available on request.

Acknowledgements

This research has been funded by the Royal Society through a Newton International Fellowship (NIF\R1\192806). The initial construction of the OSL scanning imaging system was funded by the Food Standard Agency through the project CSA 5240. The authors are thankful to Frances Pearce from Landauer for providing the dosimeter sheet.

References

Agostinelli, S., Allison, J., Amako, K., Apostolakis, J., Araujo, H., Arce, P., Asai, M., Axen, D., Banerjee, S., Barrand, G., Behner, F., Bellagamba, L., Boudreau, J., Broglia, L., Brunengo, A., Burkhardt, H., Chauvie, S., Chuma, J., Chytracek, R., Cooperman, G., Cosmo, G., Degtyarenko, P., Dell'Acqua, A., Depaola, G., Dietrich, D., Enami, R., Feliciello, A., Ferguson, C., Fesefeldt, H., Folger, G., Foppiano, F., Forti, A., Garelli, S., Giani, S., Giannitrapani, R., Gibin, D., Cadenas, J. J. Gomez, Gonzlez, I., Abril, G. Gracia, Greeniaus, G., Greiner, W., Grichine, V., Grossheim, A., Guatelli, S., Gumplinger, P., Hamatsu, R., Hashimoto, K., Hasui, H., Heikkinen, A., Howard, A., Ivanchenko, V., Johnson, A., Jones, F.W., Kallenbach, J., Kanaya, N., Kawabata, M., Kawabata, Y., Kawaguti, M., Kelner, S., Kent, P., Kimura, A., Kodama, T., Kokoulin, R., Kossov, M., Kurashige, H., Lamanna, E., Lampen, T., Lara, V., Lefebure, V., Lei, F., Liendl, M., Lockman, W., Longo, F., Magni, S., Maire, M., Medernach, E., Minamimoto, K., de Freitas, P. Mora, Morita, Y., Murakami, K., Nagamatu, M., Nartallo, R., Nieminen, P., Nishimura, T., Ohtsubo, K., Okamura, M., O'Neale, S., Oohata, Y., Paech, K., Perl, J., Pfeiffer, A., Pia, M.G., Ranjard, F., Rybin, A., Sadilov, S., Salvo, E.Di, Santin, G., Sasaki, T., Savvas, N., Sawada, Y., Scherer, S., Sei, S., Sirotenko, V., Smith, D., Starkov, N., Stoecker, H., Sulkimo, J., Takahata, M., Tanaka, S., Tcherniaev, E., Tehrani, E. Safai, Tropeano, M., Truscott, P., Uno, H., Urban, L., Urban, P., Verderi, M., Walkden, A., Wander, W., Weber, H., Wellisch, J.P., Wenaus, T., Williams, D.C., Wright, D., Yamada, T., Yoshida, H., Zschiesche, D., 2003. Geant4–a simulation toolkit. Nucl. Instrum. Methods Phys. Res. Sect. A Accel. Spectrom. Detect. Assoc. Equip. 506 (3), 250–303.

Allison, J., Amako, K., Apostolakis, J., Arce, P., Asai, M., Aso, T., Bagli, E., Bagulya, A., Banerjee, S., Barrand, G., Beck, B.R., Bogdanov, A.G., Brandt, D., Brown, J.M.C., Burkhardt, H., Canal, Ph, Cano-Ott, D., Chauvie, S., Cho, K., Cirrone, G.A.P., Cooperman, G., Cortés-Giraldo, M.A., Cosmo, G., Cuttone, G., Depaola, G., Desorgher, L., Dong, X., Dotti, A., Elvira, V.D., Folger, G., Francis, Z., Galoyan, A., Garnier, L., Gayer, M., Genser, K.L., Grichine, V.M., Guatelli, S., Guèye, P., Gumplinger, P., Howard, A.S., Hřivnáčová, I., Hwang, S., Incerti, S., Ivanchenko, A., Ivanchenko, V.N., Jones, F.W., Jun, S.Y., Kaitaniemi, P., Karakatsanis, N., Karamitros, M., Kelsey, M., Kimura, A., Koi, T., Kurashige, H., Lechner, A., Lee, S.B., Longo, F., Maire, M., Mancusi, D., Mantero, A., Mendoza, E., Morgan, B., Murakami, K., Nikitina, T., Pandola, L., Paprocki, P., Perl, J., Petrović, I., Pia, M.G., Pokorski, W., Quesada, J.M., Raine, M., Reis, M.A., Ribon, A., Ristić Fira, A., Romano, F., Russo, G., Santin, G., Sasaki, T., Sawkey, D., Shin, J.I., Strakovsky, I.I., Taborda, A., Tanaka, S., Tomé, B., Toshito, T., Tran, H.N., Truscott, P.R., Urban, L., Uzhinsky, V., Verbeke, J.M., Verderi, M., Wendt, B.L., Wenzel, H., Wright, D.H., Wright, D.M., Yamashita, T., Yarba, J., Yoshida, H., 2016. Recent developments in GEANT4. Nucl. Instrum. Methods Phys. Res. 835, 186–225.

Bailiff, I.K., 2018. An examination of beta dose attenuation effects in coarse grains located in sliced samples. Radiat. Meas. 120, 188–194. https://doi.org/10.1016/j.radmeas.2018.07.015.

Cresswell, A.J., Carter, J., Sanderson, D.C.W., 2018. Dose rate conversion parameters: assessment of nuclear data. Radiat. Meas. 120, 195–201. https://doi.org/10.1016/j.radmeas.2018.02.007.

Cunningham, A.C., Buylaert, J.-P., Murray, A.S., 2022. Beta attenuation in granular matrices: implications for trapped-charge dating. Geochronology 4, 517–531. https://doi.org/10.5194/gchron-2021-17.

Duller, G.A.T., Bøtter-Jensen, L., Murray, A.S., 2003. Combining infrared- and green-laser stimulation sources in single-grain luminescence measurements of feldspar and quartz. Radiat. Meas. 37, 543–550. https://doi.org/10.1016/S1350-4487(03)00050-7.

Endo, A., Katoh, T., Kobayashi, I., Joshi, R., Sur, J., Okano, T., 2012. Characterization of optically stimulated luminescence dosemeters to measure organ doses in diagnostic radiology. Dentomaxillofacial Radiol. 41–3, 211–216.

Fang, F., Martin, L., Williams, I., Rajabi, S., Brink, F., Mercier, N., Grün, R., 2018. 2D modeling: a new approach for assessing heterogeneous beta dose rates in luminescence and ESR dating, II: application to igneous rocks. Quat. Geochronol. 48, 195–206. https://doi.org/10.1016/j.quageo.2018.07.005.

Fleming, S.J., 1970. Thermoluminescent dating: refinement of the quartz inclusion method. Archaeometry 12, 133–143. https://doi.org/10.1111/j.1475-4754.1970.tb00016.x.

Fu, X., Romanyukha, A.A., Li, Bo, Jankowski, N.R., Lachlan, T.J., Jacobs, Z., George, S.P., Rosenfeld, A.B., Roberts, R.G., 2022. Beta dose heterogeneity in sediment samples measured using a Timepix pixelated detector and its implications for optical dating of individual mineral grains. Quat. Geochronol. 68, 101254 https://doi.org/10.1016/j.quageo.2022.101254.

Guérin, G., Mercier, N., Nathan, R., Adamiec, G., Lefrais, Y., 2012a. On the use of the infinite matrix assumption and associated concepts: a critical review. Radiat. Meas. 47, 778–785.

Guérin, G., Discamps, E., Lahaye, C., Mercier, N., Guibert, P., Turq, A., Dibble, H.L., McPherron, S.P., Sandgathe, D., Goldberg, P., Jain, M., Thomsen, K., Patou-Mathis, M., Castel, J.-C., Soulier, M.-C., 2012b. Multi-method (TL and OSL), multi-material (quartz and flint) dating of the Mousterian site of Roc de Marsal (Dordogne, France): correlating Neanderthal occupations with the climatic variability of MIS 5–3. J. Archaeol. Sci. 39, 3071–3084.

Han, Z.-Y., Li, S.-H., Tso, M.Y.W., 1999. TL dating technique based on a trap model and its application as a geochronometer for granitic quartz. Radiat. Protect. Dosim. 84, 471–478. https://doi.org/10.1093/oxfordjournals.rpd.a032780.

Ingamells, C.O., 1974. Control of geochemical error through sampling and subsampling diagrams. Geochem. Cosmochim. Acta 38, 1225–1237. https://doi.org/10.1016/0016-7037(74)90118-5.

Jenkins, G.T.H., Duller, G.A.T., Roberts, H.M., Chiverrell, R.C., Glasser, N.F., 2018. A new approach for luminescence dating glaciofluvial deposits - high precision optical dating of cobbles. Quat. Sci. Rev. 192, 263–273.

King, G.E., Herman, F., Lambert, R., Valla, P.G., Guralnik, B., 2016. Multi-OSL-thermochronometry of feldspar. Quat. Geochronol. 33, 76–87. https://doi.org/10.1016/j.quageo.2016.01.004.

Martin, L., Mercier, N., Incerti, S., Lefrais, Y., Pecheyran, C., Guerin, G., Jarry, M., Bruxelles, L., Bon, F., Pallier, C., 2015. Dosimetric study of sediments at the Beta dose rate scale : characterization and modelization with the DosiVox software. Radiat. Meas. 81, 134–141.

Martin, L., Fang, F., Mercier, N., Incerti, S., Grün, R., Lefrais, Y., 2018. 2D modelling: a Monte Carlo approach for assessing heterogeneous β Drs in luminescence and ESR dating: paper I, theory and verification. Quat. Geochronol. 48, 25–37.

Martin, L., Sanderson, D., Paling, S., Cresswell, A., Murphy, S., 2022. Advancing dosimetry for Dating Environmental Materials: development of an ultra-sensitive beta dosimeter system and potential for beta autoradiography. Radiat. Meas. 154, 106760 https://doi.org/10.1016/j.radmeas.2022.106760.

Mejdahl, V., 1983. Feldspar inclusion dating of ceramics and burnt stones. Council Europe J. PACT 9, 351–364.

Murphy, A., Paling, S., 2012. The Boulby mine underground science facility: the search for dark matter, and beyond. Nucl. Phys. News 22 (1), 19–24. https://doi.org/10.1080/10619127.2011.629920.

Murray, A.S., Roberts, R.G., 1997. Determining the burial time of single grains of quartz using optically stimulated luminescence. Earth Planet Sci. Lett. 152, 163–180. https://doi.org/10.1016/S0012-821X(97)00150-7.

Nathan, R.P., Thomas, P.J., Jain, M., Murray, A.S., Rhodes, E.J., 2003. Environmental dose rate heterogeneity of beta radiation and its implications for luminescence dating: Monte Carlo modelling and experimental validation. Radiat. Meas. 37, 305–313.

Plachy, A.L., Sutton, S.R., 1982. Determination of the dose-rate to quartz in granite. PACT 6, 188–194.

Rades, E.F., Sohbati, R., Lüthgens, C., Jain, M., Murray, A.S., 2018. First luminescence-depth profiles from boulders from moraine deposits: insights into glaciation chronology and transport dynamics in Malta valley, Austria. Radiat. Meas. 120, 281–289. https://doi.org/10.1016/j.radmeas.2018.08.011.

Rasband, W.S., 2012. ImageJ. U.S. National Institutes of Health, Bethesda, Maryland, USA. imagej.nih.gov/ij/.

Richardson, W.H., 1972. Bayesian-based iterative method of image restoration. J. Opt. Soc. Am. 62, 55–59. https://doi.org/10.1364/JOSA.62.000055.

Romanyukha, A.A., Cunningham, A.C., George, S.P., Guatelli, S., Petasecca, M., Rosenfeld, A.B., Roberts, R.G., 2017. Deriving spatially resolved beta dose rates in sediment using the Timepix pixelated detector. Radiat. Meas. 106, 483–490. https://doi.org/10.1016/J.RADMEAS.2017.04.007.

Rufer, D., Preusser, F., 2009. Potential of autoradiography to detect spatially resolved radiation patterns in the context of trapped charge dating. Geochronometria 34, 1–13.

Sage, D., Donati, L., Soulez, F., Fortun, D., Schmit, G., Seitz, A., Guiet, R., Vonesch, C., Unser, M., 2017. DeconvolutionLab2 : an Open-Source Software for deconvolution microscopy methods. Image Processing for Biologists 115, 2017.

Sanderson, D.C.W., Placido, F., Tate, J.O., 1988. Scottish vitrified forts : TL results from six study sites. Nucl. Tracks Radiat. Meas. 14, 307–316. https://doi.org/10.1016/1359-0189(88)90081-7.

Sanderson, D.C.W., Carmichael, L.A., Murphy, S., Whitely, V., Scott, E.M., Cresswell, A., 2001. Statistical and Imaging Methods for Luminescence Detection of Irradiated Ingredients. Food Standards Agency, London. Project CSA 5240. http://eprints.gla.ac.uk/58359.

Schneider, C.A., Rasband, W.S., Eliceiri, K.W., 2012. NIH Image to ImageJ: 25 years of image analysis. Nat. Methods 671. https://doi.org/10.1038/nmeth.2089.

Scott, E.M., Sanderson, D.C.W., 1988. Statistics and the additive dose method in TL dating. Nucl. Tracks Radiat. Meas. 14, 345–354. https://doi.org/10.1016/1359-0189(88)90087-8.

Sellwood, E.L., Kook, M., Jain, M., 2022. Investigating the potential of rock surface burial dating using IRPL and IRSL imaging. Radiat. Meas. 155, 106783 https://doi.org/10.1016/j.radmeas.2022.106783.

Semikolennykh, D.V., Cunningham, A.C., Kurbanov, R.N., Panin, A.V., Zolnikov, I.D., Deev, E.V., Murray, A.S., 2022. Dating of megaflood deposits in the Russian Altai using rock surface luminescence. Quat. Geochronol. 73, 101373 https://doi.org/10.1016/j.quageo.2022.101373.

Smedley, R.K., Buylaert, J.-P., Újvári, G., 2019. Comparing the accuracy and precision of luminescence ages for partially-bleached sediments using single grains of K-feldspar and quartz. Quat. Geochronol. 53, 101007 https://doi.org/10.1016/j.quageo.2019.101007.

Smedley, R.K., Duller, G.A.T., Rufer, D., Utley, J.E.P., 2020. Empirical assessment of beta dose heterogeneity in sediments: implications for luminescence dating. Quat. Geochronol. 56, 101052 https://doi.org/10.1016/j.quageo.2020.101052.

Stalder, N.F., Biswas, R.H., Herman, F., 2022. Maximized erosion at the last glacial maximum revealed by thermoluminescence thermochronometry. Quat. Geochronol. 73, 101405 https://doi.org/10.1016/j.quageo.2022.101405.

Vafiadou, A., Murray, A., Liritzis, I., 2007. Optically stimulated luminescence (OSL) dating investigations of rock and underlying soil from three case studies. J. Archaeol. Sci. 34, 1659–1669. https://doi.org/10.1016/j.jas.2006.12.004.

Zhang, M., Chen, Q., Li, X.-F., O'Donoghue, J., Ruan, S., Zanzonico, P., Ling, C.C., Humm, J.L., 2008. Image deconvolution in digital autoradiography: a preliminary study. Med. Phys. 35, 522–530. https://doi.org/10.1118/1.2828198.